

# Double-diffusive convection in a rotating cylindrical annulus with conical caps

Radostin D. Simitev

*School of Mathematics and Statistics, University of Glasgow – Glasgow G12 8QW, UK, EU*

---

## Abstract

Double-diffusive convection driven by both thermal and compositional buoyancy in a rotating cylindrical annulus with conical caps is considered with the aim to establish whether a small fraction of compositional buoyancy added to the thermal buoyancy (or vice versa) can significantly reduce the critical Rayleigh number and amplify convection in planetary cores. It is shown that the neutral surface describing the onset of convection in the double-buoyancy case is essentially different from that of the well-studied purely thermal case, and does indeed allow the possibility of low-Rayleigh number convection. In particular, isolated islands of instability are formed by an additional “double-diffusive” eigenmode in certain regions of the parameter space. However, the amplitude of such low-Rayleigh number convection is relatively weak. At similar flow amplitudes purely compositional and double-diffusive cases are characterized by a stronger time dependence compared to purely thermal cases, and by a prograde mean zonal flow near the inner cylindrical surface. Implications of the results for planetary core convection are briefly discussed.

*Keywords:* double-diffusive convection, buoyancy-driven instabilities, planetary core

---

## 1. Introduction

Convection in the cores of the Earth and the terrestrial planets is of significant interest as it drives the dynamo processes that generate and sustain the global magnetic fields of these bodies (Kono and Roberts, 2002; Jones, 2007). Core convection is a double-diffusive process driven by density variations due to non-uniform temperature and composition (Braginsky and Roberts, 1995). While double-diffusive phenomena are well-studied in oceanography, metallurgy, mantle convection and other contexts (Huppert and Turner, 1981; Turner, 1974, 1985; Schmitt, 1994), their manifestations in core convection remain poorly understood. It is thought that thermal and compositional buoyancy in the Earth’s core have comparable strength (Lister and Buffett, 1995; Nimmo, 2007), and that temperature and concentration of light elements have widely different molecular diffusive time scales, boundary conditions and source-sink distributions (Braginsky and Roberts, 1995). Yet, most planetary and geo-dynamo models consider only thermal convection or, at best, lump temperature and concentration into a single “codensity” variable. The last approach is poorly justified, as it is only valid for equal diffusivities and identical boundary conditions. Indeed, while eddy diffusivities due to small-scale turbulent mixing tend to attain similar values, the turbulence in many cases, e.g. weakly-convecting stratified layers, may not be as fully developed to wipe out the large differences in molecular diffusivities (Busse and Simitev, 2011). At the same time, relatively small variations in diffusivity ratios may have significant dynamical effects (e.g. Simitev and Busse, 2005). So far, only few studies have been published where

thermal and compositional buoyancy are considered separately. Cardin and Olson (1992) performed an experimental investigation of thermochemical convection in rotating spherical shell. A double-diffusive numerical dynamo model with a partly stable thermal gradient and destabilizing compositional component has been recently studied by Manglik et al. (2010), as a situation likely applicable to Mercury. Various driving scenarios where thermal and compositional gradients are both destabilizing have been explored numerically by Breuer et al. (2010). All of these papers report significant differences in their results to the single-diffusive (codensity) case and emphasize the need for further investigation. The onset of double-diffusive convection in an axisymmetric rotating system has been studied by Busse (2002b) in certain asymptotic limits, and it was found that a small fraction of compositional buoyancy could significantly reduce the critical Rayleigh number, and thus amplify core convection. This prediction is potentially very important, as it may shed light on the thermodynamic state of the core and the energy budget of the geodynamo. However, concerted numerical simulations have so far failed to confirm it (Breuer et al., 2010).

With this motivation, the goals of this letter are to establish the possibility of low-Rayleigh number double-diffusive convection, and to elucidate the mechanisms by which thermal and compositional buoyancy interact. To this end, a simple model of a rotating cylindrical annulus with conical end caps is considered here. This model has been very useful in capturing the basic behaviour of nearly geostrophic convection in the equatorial regions of planetary cores (Busse, 2002a; Jones, 2007) and offers significant mathematical and computational advantages. The attention is restricted here to the effects induced by the difference in diffusivity values, while the more realistic cases of distinct boundary conditions and source-sink distribu-

---

*Email address:* Radostin.Simitev@glasgow.ac.uk (Radostin D. Simitev)

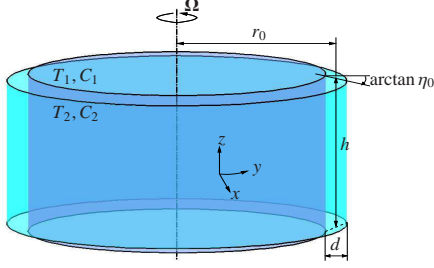


Figure 1: Sketch of the rotating cylindrical annulus with conical end caps. Note that the sketch is not to scale with the limits of a small gap and a small angle of inclination of the conical caps.

tions are disregarded at present. The mathematical formulation and the methods of solution are presented in Section 2. Sections 3 and 4 describe linear and finite-amplitude properties of double-diffusive convection. Conclusions and possible implications for planetary cores are discussed in Section 5.

## 2. Formulation and methods of solution

A cylindrical annulus with conical caps full of a two-component fluid, and rotating about its axis of symmetry with an angular velocity  $\Omega$  is considered. The configuration is shown in figure 1, and a mathematical formulation of the problem given earlier by Busse (1986, 2002b) is adopted. In particular, the inner and outer cylindrical walls are kept at constant temperatures  $T_0 \mp \Delta T/2$ , and at constant values of the concentration of the light element  $C_0 \mp \Delta C/2$ , respectively, such that a density gradient opposite to the direction of the centrifugal force is established as the basic state of the system. The effect of the centrifugal force is similar to that of gravity in self-gravitating spheres and shells in that the buoyancy-driven motions occur in the same way as in the case when the force and the gradients of temperature and concentration are reversed. This formulation has the important advantage of being amenable to experimental realizations (e.g., Busse and Carrigan, 1974). The gap width  $d$  of the annulus is used as a length scale,  $d^2/\nu$  – as the time scale, and  $\nu\Delta T/\kappa$  and  $\nu\Delta C/\kappa$  – as the scales of temperature and concentration of light material, respectively. Here  $\nu$  is the kinematic viscosity, and  $\kappa$  is the thermal diffusivity. A small-gap approximation,  $d/r_0 \ll 1$ , is assumed, where  $r_0$  is the mean radius. This makes it possible to neglect the spatial variations of the centrifugal force, and of the temperature and concentration gradients of the static state, and to introduce a Cartesian system of coordinates with the  $x$ -,  $y$ -, and  $z$ -coordinates in the radial, azimuthal and axial directions, respectively. The Boussinesq approximation is adopted, in that the variation of density,

$$\rho = \rho_0(1 - \gamma_t\Delta T(x - \Theta/P) - \gamma_s\Delta C(x - \Gamma/L)), \quad (1)$$

is only taken into account in connection with the body forces acting on the fluid. Here,  $\gamma_t$  and  $\gamma_s$  are the coefficients of thermal and chemical expansion, and the other symbols are defined below. The linear dependence on  $x$  is unrealistic for the concentration as it requires zero-concentration boundary conditions (5). A more realistic zero-flux condition would make the problem rather involved (Braginsky and Roberts, 1995) and

will divert from the main focus of this paper which is to investigate the influence of diffusivities isolated from the effects of boundary conditions. A discussion of different types of boundary conditions related to core convection and the geodynamo can be found, for example, in (Kutzner and Christensen, 2002; Busse and Simitev, 2006). Assuming a small angle of inclination of the conical end caps with respect to the equatorial plane, and taking into account that the annulus is rotating, the velocity obeys approximately the Proudman-Taylor theorem and can be described in first approximation by its geostrophic part

$$\mathbf{u} = \nabla \times \mathbf{k}\psi(x, y, t) + O(\eta_0), \quad (2)$$

where  $\eta_0 \ll 1$  is the tangent of the said angle. Averaging over  $z$ , the governing equations for the leading order of the dimensionless deviations of the temperature  $\Theta$ , the concentration  $\Gamma$ , and the stream function  $\psi$  from the static state of no flow can be written in the 2D cartesian form (Busse, 2002b)

$$\begin{aligned} ((\partial_t - \nabla^2) + \mathcal{J}_\psi)\nabla^2\psi - \eta^*\partial_y\psi + \partial_y(R_t\Theta + R_s\Gamma) &= 0, \\ P(\partial_t + \mathcal{J}_\psi)\Theta - \nabla^2\Theta + \partial_y\psi &= 0, \\ P(\partial_t + \mathcal{J}_\psi)\Gamma - L^{-1}\nabla^2\Gamma + \partial_y\psi &= 0, \end{aligned} \quad (3)$$

where  $\mathcal{J}_\psi = (\partial_x\psi)\partial_x - (\partial_x\psi)\partial_y$ , and the definitions of the rotation rate, Prandtl, Lewis, thermal and compositional Rayleigh numbers  $\eta^*$ ,  $P$ ,  $L$ ,  $R_t$ , and  $R_s$  are

$$\begin{aligned} \eta^* &= \frac{4\eta_0\Omega d^3}{h\nu}, & P &= \frac{\nu}{\kappa}, & L &= \frac{\kappa}{D}, \\ R_t &= \frac{\gamma_t d^3 g \Delta T}{\nu\kappa}, & R_s &= \frac{\gamma_s d^3 g \Delta C}{\nu\kappa}, \end{aligned} \quad (4)$$

respectively. Here,  $D$  is the diffusivity of the light material,  $h$  is the axial length of the annulus, and  $g = \Omega^2 r_0$  is the average centrifugal acceleration analogous to gravitational acceleration. Fixed temperature and concentration, and stress-free BCs for the velocity are assumed at  $x = \pm 1/2$ ,

$$\psi = \partial_x^2\psi = \Theta = \Gamma = 0 \quad \text{at} \quad x = 1/2, \quad (5)$$

while periodicity is imposed in the  $y$ -direction. For further details on the assumptions and for evidence of the utility of this model to capture the dynamics of convection in rotating spherical shells, the reader is referred to the reviews of Busse (2002a); Jones (2007) and the references cited therein.

The linearized version of equations (3) allows an analytical solution. The nonlinear equations (3) are solved numerically by a modification of the Galerkin spectral method used previously by Or and Busse (1987); Schnaubelt and Busse (1992). The dependent variables  $\psi$ ,  $\Theta$  and  $\Gamma$  are expanded in functions satisfying the boundary conditions

$$\begin{pmatrix} \psi \\ \Theta \\ \Gamma \end{pmatrix} = \sum_{l=0, n=1}^{\infty} \begin{bmatrix} \hat{a}_{ln}(t) \\ \hat{b}_{ln}(t) \\ \hat{c}_{ln}(t) \end{bmatrix} \cos(n\beta y) + \begin{bmatrix} \check{a}_{ln}(t) \\ \check{b}_{ln}(t) \\ \check{c}_{ln}(t) \end{bmatrix} \sin(n\beta y) \times \sin(l\pi(x + 1/2)). \quad (6)$$

After projecting equations (3) onto the respective expansion functions, a system of nonlinear ordinary differential equations

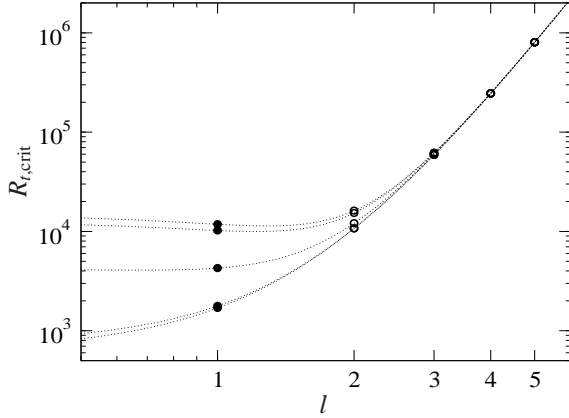


Figure 2: The critical Rayleigh number  $R_{t,\text{crit}}$  of purely-thermal convection as a function of the radial wave number  $l$  for  $\alpha = 5$ ,  $\eta^* = 600$ ,  $R_s = 0$ , and  $P = 10^{-2}, 10^{-1}, 1, 10, 10^2$  (from bottom to top). The solid circles indicate the preferred values of  $l$ .

is obtained for the unknown coefficients  $\hat{a}_{ln}(t)$ ,  $\check{a}_{ln}(t)$ ,  $\hat{b}_{ln}(t)$ ,  $\check{b}_{ln}(t)$ ,  $\hat{c}_{ln}(t)$  and  $\check{c}_{ln}(t)$ . The system is integrated in time by a combination of an Adams-Bashforth scheme for the nonlinear terms and a Crank-Nicolson scheme for the diffusion and the other linear terms. A truncation scheme must be introduced in practice: the equations and the corresponding coefficients are neglected when  $l > N_x$  and  $n > N_y$ , where the truncation parameters  $N_x$  and  $N_y$  must be sufficiently large so that the physical properties of the solution do not change significantly when their values are increased. The computations reported in the following have been done with  $\beta = 1$ ,  $N_x = 35$  and  $N_y = 55$ .

### 3. The linear onset of double-diffusive convection

Without loss of generality, small perturbations about the state of no motion can be assumed to take the form

$$(\psi, \Theta, \Gamma)^T = (\tilde{\psi}, \tilde{\Theta}, \tilde{\Gamma})^T \sin(l\pi(x + 1/2)) e^{i\alpha y + \lambda t}, \quad (7)$$

where  $\alpha$  and  $l$  denote the azimuthal and the radial wave numbers,  $\lambda = \sigma + i\omega$ , with  $\sigma \in \mathbb{R}$  and  $\omega \in \mathbb{R}$  being the growth rate and the frequency of oscillations, respectively. The superscript  $\top$  denotes transposition, and  $(\tilde{\psi}, \tilde{\Theta}, \tilde{\Gamma})^T$  is a constant component vector. Then, the linearised version of equations (3) reduces to a matrix eigenvalue problem for  $\lambda$  and  $(\tilde{\psi}, \tilde{\Theta}, \tilde{\Gamma})^T$ ,

$$\begin{pmatrix} -\frac{a^2 + i\alpha\eta^*}{a^2} & i\frac{\alpha R_t}{a^2} & i\frac{\alpha R_s}{a^2} \\ -i\frac{\alpha}{P} & -\frac{a^2}{P} & 0 \\ -i\frac{\alpha}{P} & 0 & -\frac{a^2}{PL} \end{pmatrix} \begin{pmatrix} \tilde{\psi} \\ \tilde{\Theta} \\ \tilde{\Gamma} \end{pmatrix} = \lambda \begin{pmatrix} \tilde{\psi} \\ \tilde{\Theta} \\ \tilde{\Gamma} \end{pmatrix}, \quad (8)$$

where  $a^2 = l^2\pi^2 + \alpha^2$ . In the rest of this section attention is restricted to a single-roll convective structure in radial direction by setting  $l = 1$ . Equatorially-attached ‘‘multicellular’’ thermal convection has been previously found in shells and annuli of finite gaps and convexly curved caps (e.g. Ardes et al., 1997; Plaut and Busse, 2005). However, these geometries are quite

different from the small-gap limit considered here as they provide radially inhomogeneous conditions for convection. Figure 2 demonstrates that, in the small-gap limit and for the parameter values discussed below,  $l = 1$  is always the preferred radial mode for the onset of thermal convection; the nonlinear results of section 4 further confirm the  $l = 1$  assumption.

The solution to problem (8) can be found in analytical form, and figure 3 shows the growth rate of the perturbations,  $\sigma = \text{Re}(\lambda)$ , as a function of the thermal Rayleigh number  $R_t$  for fixed values of the other parameters. The eigenmodes of purely thermal convection are also shown in the figure for comparison. Because the matrix in (8) is of size  $3 \times 3$ , it can have up to three distinct eigenmodes for typical parameter values. The analogous eigenvalue problem for purely thermal convection has a matrix of size  $2 \times 2$  that can have up to 2 eigenmodes at most. Thus, a basic distinction between purely thermal and double-buoyancy convection is the appearance of an additional ‘‘double-diffusive’’ eigenmode. The remaining two modes are analogous to the two possible modes of purely thermal convection, as figure 3 clearly demonstrates. In figure 3 and in the following, these three possible modes are denoted by **aDD** (additional Double-Diffusive mode), **uTL** (unstable Thermal-Like mode), and **sTL** (stable Thermal-Like mode). The **aDD** mode becomes unstable for smaller values of  $R_t$  compared to the **uTL** mode. This provides a possibility for low-Rayleigh number convection as suggested by Busse (2002b). The growth rate of the **aDD** mode is a non monotonic function of  $R_t$ , and it is remarkable that in the case of a destabilizing compositional gradient ( $R_s > 0$ ), the **aDD** mode regains stability before the **uTL** mode becomes unstable. This limits the parameter space where low-Rayleigh number convection occurs, and indicates the existence of isolated regions of instability.

The regions of linear stability ( $\sigma < 0$ ) and instability ( $\sigma > 0$ ) in the parameter space are separated from each other by a neutral surface. It is defined in implicit form by the characteristic equation of the eigenvalue problem (8) where  $\sigma = 0$ ,

$$(i\omega P + a^2)(i\omega P + a^2/L)((i\omega + a^2)a^2 + i\alpha\eta^*) - \alpha^2 R_t (i\omega P + a^2/L) - \alpha^2 R_s (i\omega P + a^2) = 0. \quad (9)$$

Following Busse (2002b), this equation is split into real and imaginary parts from which the frequency of oscillations  $\omega$  and the critical value of any parameter of the problem as a function of the remaining ones can be found in explicit analytical form. Here, the thermal Rayleigh number  $R_t$  is chosen as the principal control parameter, because it offers the possibility of direct comparison with the well-studied purely thermal case. The five-dimensional neutral surface,  $R_t = R_t(P, \eta^*, L, R_s, \alpha)$ , is represented graphically by its projections (neutral curves) onto the planes  $\alpha - R_t$ ,  $R_s - R_t$ ,  $\eta^* - R_t$ , and  $P - R_t$  in panels (a, b, c, d) of figure 4 respectively, for fixed values of the remaining parameters of the problem. The dependence on the Lewis number  $L$  is shown in the form of contour lines in this figure thus exhausting all possible parameter dependencies. The same approach is adopted to represent the corresponding frequency  $\omega = \omega(P, \eta^*, L, R_s, \alpha)$  in figure 5, where  $|\omega|$  is plotted instead to allow visualisation of finer details in the plots. The most

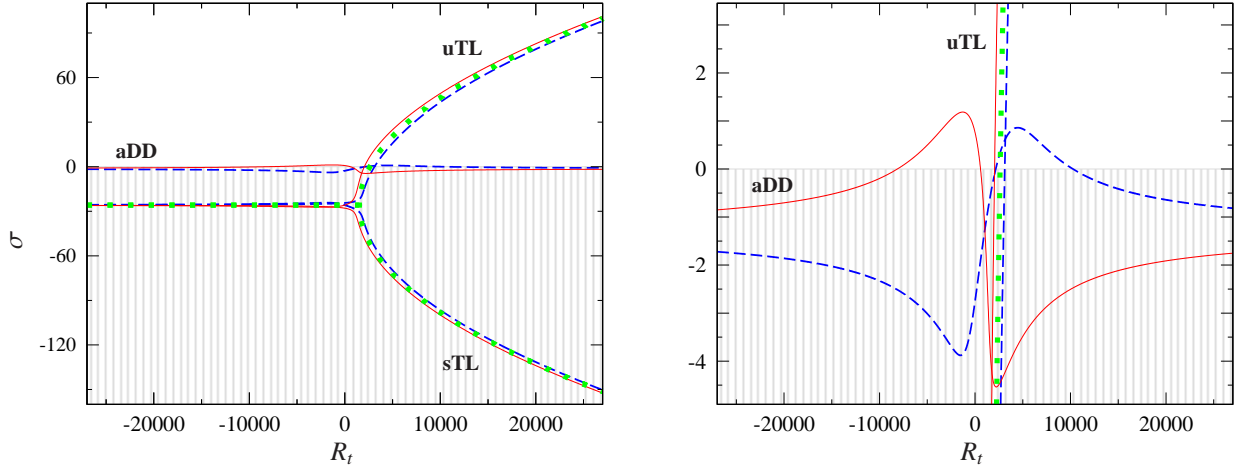


Figure 3: (Color online.) The growth rates,  $\sigma = \text{Re}(\lambda)$ , of the eigenmodes of double-diffusive convection in the rotating annulus geometry as a function of the thermal Rayleigh number  $R_t$  at  $P = 1$ ,  $\eta^* = 400$ ,  $\alpha = 4$ ,  $L = 20$ ,  $R_s = 500$  (solid red line) of  $R_s = -500$  (dashed blue line). The three possible modes are denoted by **aDD**, **uTL**, and **sTL** in the example of  $R_s = 500$ . The basic state of no flow is linearly stable in the shaded region where the growth rate is negative. Convection sets in the non-shaded region. The green dotted lines correspond to the well-studied purely thermal modes of convection e.g. (Busse, 1986) at the same parameter values (and  $R_s = 0$ ,  $L$  - arbitrary). The right panel is identical to the left one, only the scale of the y axis is enlarged to show finer details.

prominent feature of the neutral curves is that they are multi-valued, and may split into closed, entirely isolated branches. This can be understood from the fact that the dispersion relation (9) is a linear equation in  $R_t$ , and a cubic equation in  $\omega$ , so it has either one, two or three real roots as its discriminant takes negative, zero and positive values when parameter values are continuously varied. The stability of the basic state in the various regions formed thereby can be determined from the sign of the growth rate  $\sigma$  as described in relation to figure 3. For example in the case  $L = 30$  of figure 4, convection occurs within the regions that have been shaded.

The topology of the neutral curves of double-diffusive convection is essentially different from that in the case of purely thermal convection, also shown in figure 4. While in the latter case for fixed values of the other parameters there is one and only one critical value of  $R_t$  above which convection occurs, in the former case up to three values of  $R_t$  are needed to specify stability criteria due to the multi-valued nature of the neutral curves. Note that the critical wave numbers associated with each of the three distinct critical values of  $R_t$  are also different as seen in figure 4(a). Occurrence of isolated regions of secondary instability has been reported in the case of quasi-geostrophic purely thermal convection by Plaut and Busse (2002). Note, that this is quite different from the isolated regions of primary instability discussed in this paper. It is likely that the double-diffusive case will exhibit even more complex behaviour in its transition to tertiary states, and this will be subject for future study. Neutral curves with similar complex topology have been previously reported in unrelated situations, e.g. a differentially heated inclined box (Hart, 1971), quiescent layers with density dependent on two or more stratifying agencies with different diffusivities (Pearlstein, 1981), isothermal shear flows (Meseguer and Marques, 2002), buoyancy-driven flows in an inclined layer (Chen and Pearlstein, 1989), and penetrative convection in porous media (Straughan and Walker, 1997).

It is of interest to discuss the expressions

$$R_t^{(1)} = \left[ \frac{a^6}{\alpha^2} + \frac{1}{a^2} \left( \frac{\eta^* P}{1+P} \right)^2 \right] - \frac{a^2 R_s^2}{\eta^{*2} P} - \frac{2PR_s}{1+P}, \quad (10)$$

$$\omega^{(1)} = -\frac{\eta^* \alpha}{a^2(1+P)} + \frac{aR_s}{\eta^* P},$$

and

$$R_t^{(2)} = \frac{a^6}{\alpha^2} - \frac{a^2}{\eta^{*2} P} R_s^2, \quad (11)$$

$$\omega^{(2)} = -\frac{aR_s}{\eta^* P} \left[ 1 + \frac{a^2 R_s (1+P)}{\eta^{*2} P} \right],$$

derived by Busse (2002b) as solutions to the dispersion relation (9) in the asymptotic limit of large  $L$ . The first root corresponds to the well-studied thermal Rossby waves, (e.g. Busse, 1986), modified by the presence of the second buoyancy component and describes the onset of the **uTL** mode. The physical nature of the second root (“the slow mode”) can be understood from the observation that in the limit of large  $\eta^*$  the second term in (11) vanishes and the critical Rayleigh number for the onset of Rayleigh-Bénard convection in a non-rotating plane layer is recovered (Busse, 2002b). Thus, the additional buoyancy provided by the compositional gradient,  $R_s \partial_y \Gamma$ , counteracts the unbalanced part of the convection-inhibiting Coriolis force,  $\eta^* \partial_y \psi$ , in equations (3). Expressions (10) and (11) are shown in figures 4 and 5, and it can be seen that they provide a good approximation to some pieces of the neutral curves even for moderate and small values of  $L$  and  $\eta^*$ . It has been implicitly assumed by Busse (2002b) that there is a unique critical Rayleigh number above which convection sets in. This led to the conclusion that the slow mode is the one preferred at onset, as  $R_t^{(2)}$  is always smaller than  $R_t^{(1)}$ . The presented results show that this assumption is not always correct, and that the multi-valued nature of the neutral curves must be taken into account.

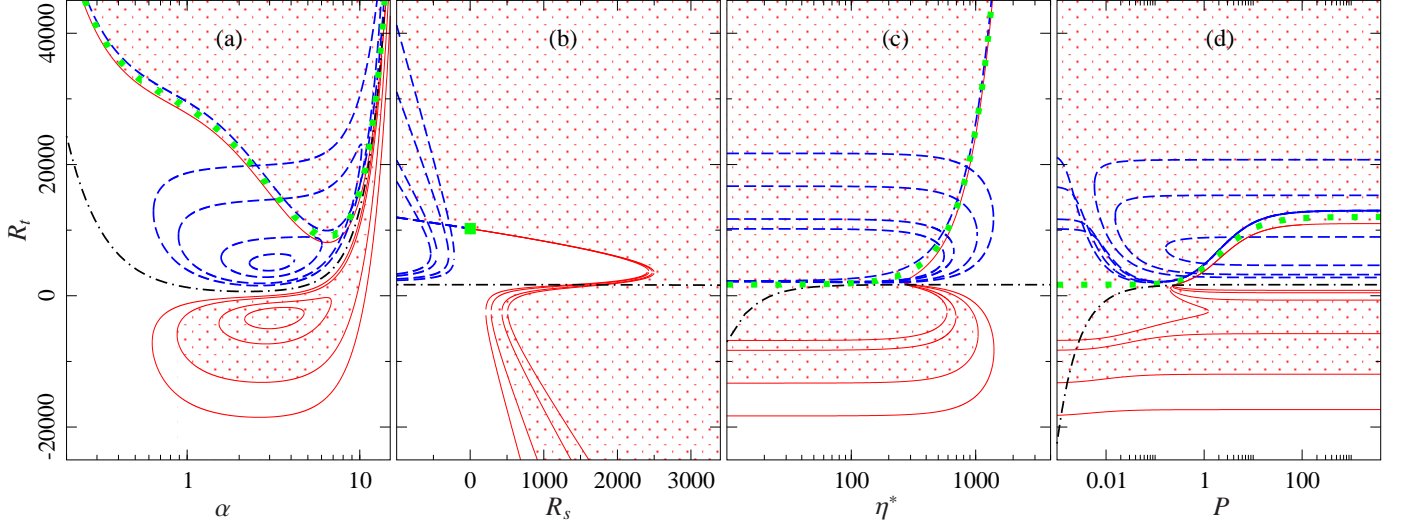


Figure 4: (Color online.) Neutral curves of double-diffusive convection in the rotating annulus geometry. Projections of the neutral surfaces onto (a) the  $\alpha - R_t$  plane, (b) the  $R_s - R_t$  plane, (c) the  $\eta^* - R_t$  plane, and (d) the  $P - R_t$  plane. In all panels, the values of  $\alpha = 5$ ,  $P = 10$ ,  $\eta^* = 600$ ,  $R_s = -500$  (thick dashed blue lines) and  $R_s = 500$  (thin solid red lines), and  $L = 17$  (innermost contour), 20, 30, 40 are kept fixed, except where they are given on the abscissa. As an example, the linearly unstable regions are shaded in the case  $R_s = 500$ ,  $L = 30$ ; the other curves form similar regions as well. The thick dotted green lines (a single point in panel (b)) correspond to the well-known purely thermal Rossby wave modes of convection e.g. (Busse, 1986) at the same parameter values (and  $R_s = 0$ ,  $L$ -arbitrary), and approximate closely the first asymptotic root (10). The black dash-dotted line represents the second asymptotic root (11).

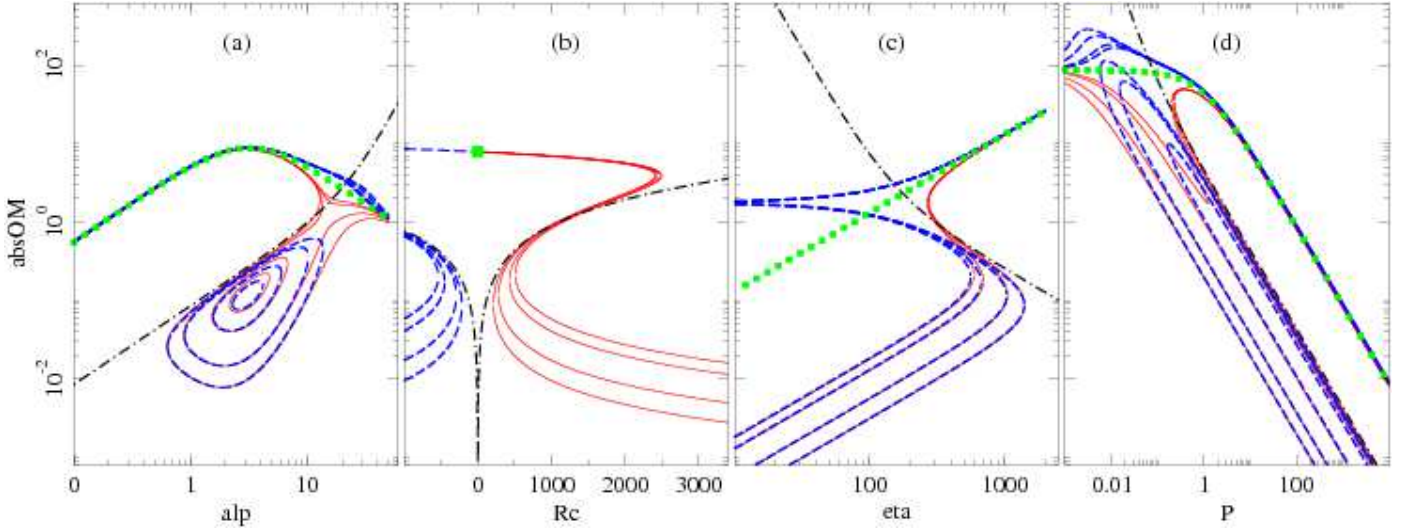


Figure 5: (Color online.) Amplitude of the frequency of oscillation,  $|\omega|$ , corresponding to the critical curves shown in figure 4. The line types and the parameter values are identical to those used in figure 4.

For example, when the concentration gradient is destabilizing,  $R_t^{(2)}$  is, actually, the value at which convection decays as  $R_t$  is increased.

#### 4. Double-diffusive convection at finite amplitudes

The linear results of section 3 demonstrate that low-Rayleigh number convection is indeed possible albeit the situation is more complicated. Below, the question whether such low-Rayleigh number flows are sufficiently vigorous to generate magnetic field is addressed and finite-amplitude properties of

double-diffusive convection are explored. Finite-amplitude solutions are characterized by their mean zonal flow, stream function, temperature and concentration perturbations, defined as

$$v_0(x, t) = \langle \partial_x \psi \rangle = \partial_x \Psi_0, \quad \Theta_0(x, t) = \langle \Theta \rangle, \quad \Gamma_0(x, t) = \langle \Gamma \rangle,$$

where  $\langle f(y) \rangle = L_y^{-1} \int_0^{L_y} f(y) dy$  and  $L_y = 2\pi/\beta$  is the basic periodicity length, and by the amplitude of convection

$$A^2 = \sum_{l=1, n=1}^{N_x, N_y} (\hat{a}_{ln}^2 + \check{a}_{ln}^2).$$

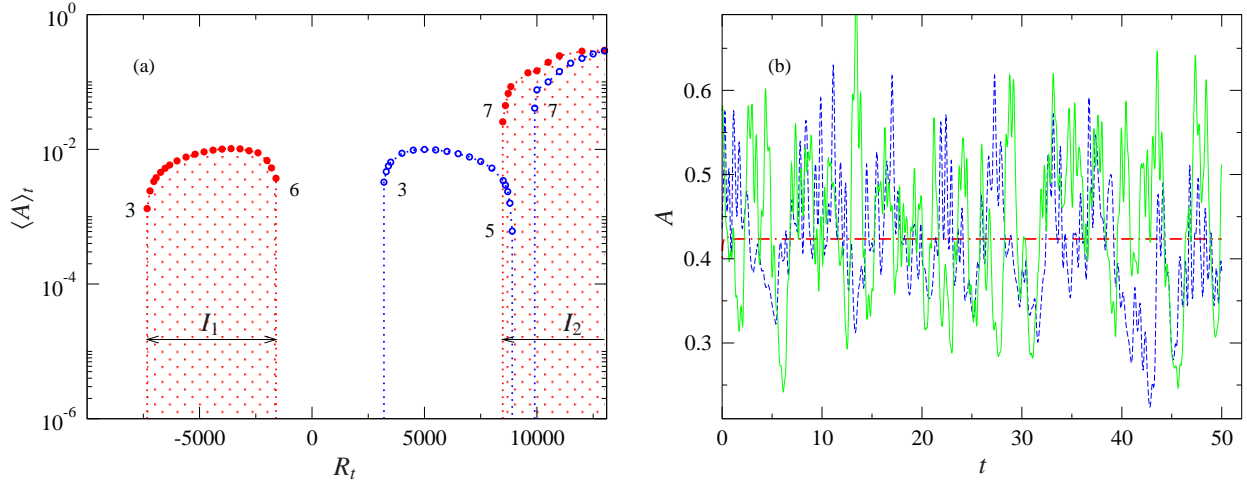


Figure 6: (Color online.) (a) The time-averaged amplitude of convection  $\langle A \rangle_t$  as a function of the thermal Rayleigh number  $R_t$  in the case  $P = 10$ ,  $L = 20$ ,  $\eta^* = 600$ , and  $R_s = 500$  (red) and  $R_s = -500$  (blue). In the case  $R_s = 500$ , the region where convection occurs is shaded. For values of  $R_t$  outside this region  $A$  is a decaying function of  $R_t$ , and the decay has been followed to values of  $A$  smaller than  $10^{-20}$  in all cases. The numbers shown near the onset of convection indicate the preferred wavenumber  $\alpha$  in each case. (b) The amplitude of convection for  $P = 10$ ,  $L = 20$ ,  $\eta^* = 600$  and  $R_t = 14050$ ,  $R_s = 0$  (Case I, red dash-dotted line),  $R_t = 0$ ,  $R_s = 17000$  (Case II, blue dashed line) and  $R_t = R_s = 9100$  (Case III, green solid line).

Figure 6(a) shows the time-averaged flow amplitude,  $\langle A \rangle_t$ , of a sequence of cases with increasing value of the thermal Rayleigh number  $R_t$  and fixed values of the remaining parameters. In full agreement with the linear theory, two regions of convection are found, labeled  $I_1$  and  $I_2$  in this figure. They are separated by a region of vanishing flow. The amplitude of convection in region  $I_1$  is more than an order of magnitude smaller than that of the flow in region  $I_2$ . Comparison with figure 3 indicates that the low-amplitude flow in  $I_1$  is associated with the **aDD** modes which are characterised by relatively small values of  $\sigma$ , while the high-amplitude convection in  $I_2$  is likely associated with the **uTL** modes. Because of its small amplitude, low-Rayleigh number double-diffusive convection in region  $I_1$  is unlikely to be able to generate and sustain magnetic fields on its own as will be further discussed below. Within region  $I_1$  all computed solutions are stationary, and for this reason not illustrated, while as  $R_t$  is increased in region  $I_2$  a sequence of stationary, time-periodic, quasi-periodic and chaotic solutions similar to those described in previous studies of purely thermal convection, e.g. (Brummell and Hart, 1993), is observed.

The additional physics introduced by the second buoyancy force makes it difficult to compare directly double-diffusive convection to the much-better studied purely thermal case. A meaningful approach for comparison is to consider cases with equally large amplitudes. This is suggested by self-consistent MHD dynamo simulations where it has been established that sufficiently vigorous turbulent flow is the primary condition for generation of self-sustained magnetic fields e.g. (Simitev and Busse, 2005; Kutzner and Christensen, 2002). For a comprehensive comparison the amplitude of the flow as a function, for instance, of the thermal and compositional Rayleigh numbers need to be computed. Then a contour plot of the data  $A(R_s, R_t)$  can be a useful comparison map as cases located on the same energy level are expected to have sim-

ilar ability for magnetic field generation. However, the practical computation of such a surface has proven too expensive even for the relatively simple annulus model considered here. For this reason, the attention is restricted below to a comparison of three representative cases: a purely thermal case, a purely compositional case, and a mixed double-diffusive case, henceforth Cases I, II and III, respectively. The time-averaged amplitudes of convection in Cases I, II and III are  $\langle A \rangle_t = 0.42, 0.42, 0.43$ , respectively. Although the values are not strictly equal, additional simulations suggest that such small differences in amplitude are not essential for the intended comparison. The three cases have destabilizing thermal and compositional gradients, which is thought to be appropriate for the Earth's core. Purposefully, the cases are moderately rather than strongly driven to illustrate how simple known properties are affected by the presence of a second buoyancy. At these amplitudes the flows considered are associated with the **uTL** modes discussed previously, rather than with the newly-found **aDD** mode. This choice is justified as the **aDD** modes do not produce sufficiently vigorous flows with interesting structure, as already discussed in relation to figure 6(a).

Figure 6(b) demonstrates that for comparable time-averaged amplitude, the purely compositional Case II and the mixed Case III have a highly chaotic time dependence while the purely thermal Case I is stationary. The spatial properties of convection are shown in figure 7 where the streamlines of the flow are plotted for the three cases along with the fluctuating parts of the temperature perturbation  $\Theta - \Theta_0$  and the concentration perturbation  $\Gamma - \Gamma_0$ . The plots represent snapshots at fixed moments in time but they have been found to be representative for the three cases. The purely thermal Case I shows a regular roll-like pattern which does not change in time, while the structures corresponding to Cases II and III are irregular and no periodic behaviour of the patterns in time can be detected. These

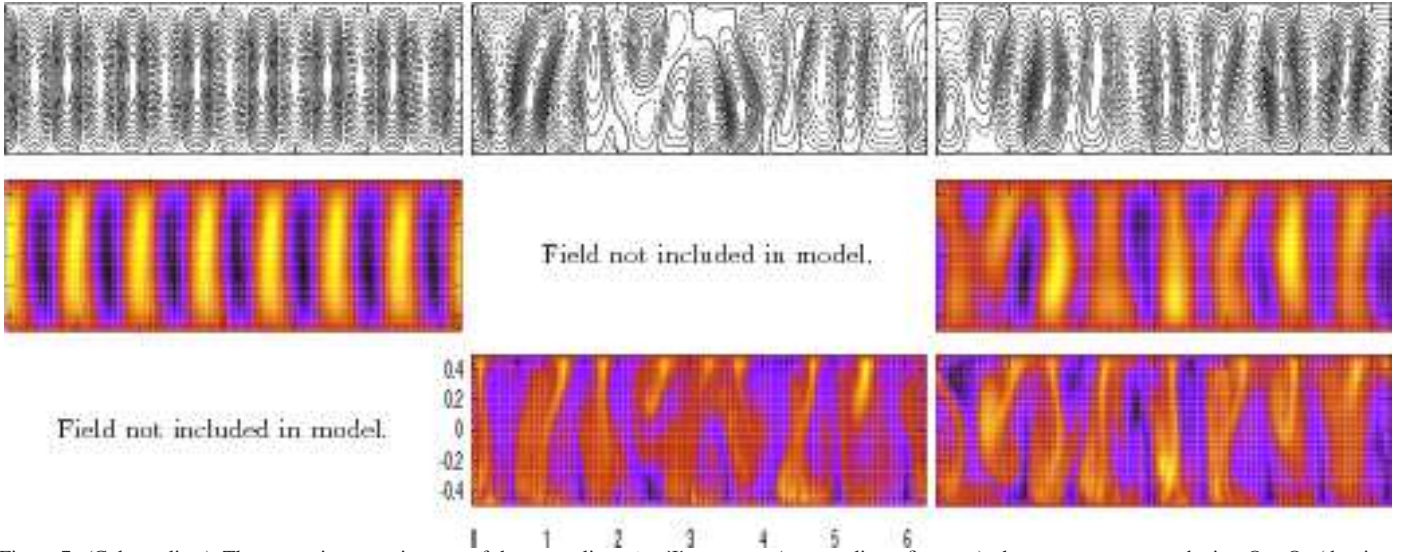


Figure 7: (Color online.) The non-axisymmetric parts of the streamlines  $\psi - \Psi_0 = \text{const.}$  (contour lines, first row), the temperature perturbation  $\Theta - \Theta_0$  (density plot, second row) and the concentration perturbation  $\Gamma - \Gamma_0$  (density plot, third row). The first, second and third columns correspond to the purely thermal Case I, to the purely compositional Case II, and to the double diffusive Case III, described in the caption of figure 6(b).

differences may be explained by the fact that Case I with ratio  $R_t/R_{t,\text{crit}} = 1.52$  is far less supercritical than Case II where  $R_s/R_{s,\text{crit}} = 17.84$ . The predominant wave number of convection appears to be the same in all three Cases, and remains equal to 7 throughout the simulations. In comparison with the temperature perturbation that shows relatively broad roll structures, the concentration perturbation forms thinner plume-like structures, consistent with the smaller compositional diffusivity. The time- and azimuthally-averaged properties of convection in the three cases are compared in figure 8. The most obvious difference is observed in the profiles of the time-averaged mean zonal flow and the Reynolds stress. These quantities are, indeed, related in that the mean flow is generated primarily by the Reynolds stress (e.g. Plaut et al., 2008; Busse, 2002b). While in the purely thermal Case I the mean flow is symmetric with respect to the mid-channel  $x = 0$ , and retrograde at its ends  $x = \pm 1/2$ , in the purely compositional Case II it is asymmetric with respect to  $x = 0$ , retrograde at  $x = 1/2$  and prograde at  $x = -1/2$ . This asymmetry can be explained by the property that, unlike in the purely thermal case, the value of  $R_s$  in the compositional case is beyond the onset of the mean-flow instability (Or and Busse, 1987). The mean flow in the mixed Case III appears similar to the purely compositional case. The remaining panels in figure 8 show that the mean properties of the mixed case are similar to the corresponding ones of the pure cases. In summary, it appears that double diffusive convection associated with the **uTL** modes can be understood on the basis of the corresponding single-diffusive cases, and that purely-thermal convection is more efficient in imprinting its properties on the overall flow even when less supercritical. This conclusion is confirmed by the experimental results of Cardin and Olson (1992) who studied thermochemical convection in rotating spherical shells and found that the structure of thermochemical flows is more like that of purely thermal convection.

## 5. Conclusion

Convection driven by density variations due to differences in temperature and concentration diffusing at different rates in a rotating cylindrical annulus with conical end caps has been studied. It is shown by a linear analysis that the neutral surface describing the onset of convection in this case has an essentially different topology from that of the well-studied purely thermal case. In particular, due to an additional “double-diffusive” eigenmode (**aDD**), neutral curves are typically multi-valued and form regions of instability in the parameter space which may be entirely disconnected from each other. It is confirmed that the asymptotic expressions for the critical Rayleigh number and frequency derived by Busse (2002b) describe the onset of convection over an extended range of non-asymptotic parameter values but do not capture the full complexity of the neutral curves. The results necessitate a revision of the assumption that there is a unique critical value of the control parameter, e.g.  $R_t$ , and call for a better appreciation of the multivalued nature of the critical curves. It is been found that finite-amplitude low-Rayleigh number convection due to **aDD** modes is possible over a wide parameter range. However, the resulting flow amplitudes are significantly lower than those of due to the familiar **uTL** modes of convection. For this reason, low-Rayleigh number flows are unlikely to be able to generate and sustain magnetic fields on their own. In order to address a more geophysically relevant situation, the nonlinear properties of convection are then investigated in the case when both driving agencies are destabilizing and produce sufficiently vigorous flow. It is proposed that a meaningful approach for direct comparison of finite-amplitude double-diffusive convection and the better studied single-diffusive case is to compare flows with equally large kinetic energies. Using this criterion the characteristics of a purely thermal case, a purely compositional case and a mixed driving case are compared. As similar flow amplitudes purely compositional and double-diffusive cases are characterized by

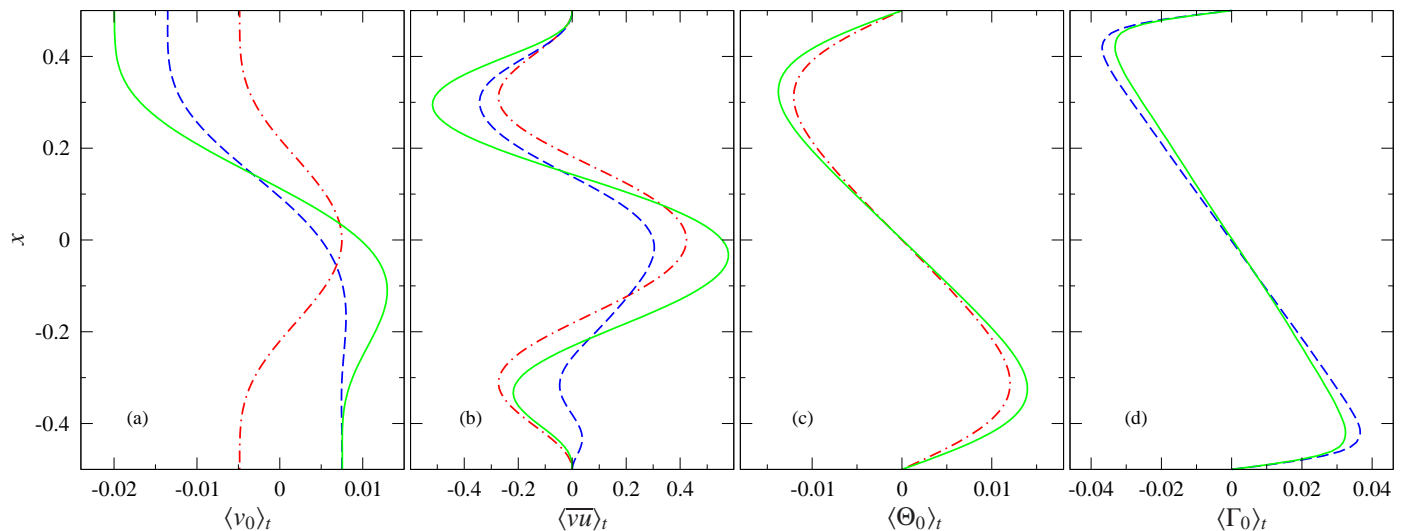


Figure 8: (Color online.) Profiles of the time-averaged (a) mean velocity  $\langle v_0 \rangle_t$ , (b) Reynolds stress  $\langle \overline{vu} \rangle_t$ , (c) mean temperature perturbation  $\langle \Theta_0 \rangle_t$ , and (d) the mean concentration perturbation  $\langle \Gamma_0 \rangle_t$ . Red dash-dotted lines indicate Case I, blue dashed lines indicate Case II, and green solid lines indicate Case III, described in the caption of figure 6(b).

a stronger time dependence compared to purely thermal cases, and by prograde mean zonal flow near the inner cylindrical surface. It is argued that double-diffusive cases may be understood on the basis of purely driven ones.

Although, its low amplitude is likely to prevent double-diffusive convection at values of the Rayleigh number significantly lower than those for single-diffusive convection from generating magnetic fields in the bulk of planetary cores, it is tempting to speculate that this type of flow may have important effects in stratified layers located just under the core-mantle boundary. Several mechanisms have been suggested for the possible formation such layers, including the build-up of light elements released during inner core solidification (Braginsky, 2006), and thermal or chemical interaction between the mantle and the core (Fearn and Loper, 1981; Lister and Buffett, 1995; Buffett and Seagle, 2010). Crucially, evidence for stratification has been recently reported in seismic observations of the outer core (Helffrich and Kaneshima, 2010). Models of inert stably stratified outer layers have been found to produce magnetic fields with morphology rather dissimilar to that of the observed field because of a thermal wind that produces unfavorable zonal flows throughout the core (Stanley and Mohammadi, 2008). Inert layers, have also been found to behave like a no-slip virtual boundary for the convective motion underneath (Takehiro et al., 2010). This last finding imposes a significant constraint on the flow, as it is well known that convection structures and the morphology of the magnetic field crucially depend on the boundary conditions (Simitev and Busse, 2005; Kutzner and Christensen, 2002; Sakuraba and Roberts, 2009). The situation may be significantly different if the stratified layer is convecting (even weakly) rather than inert and the low-Rayleigh number regime  $I_1$  found here offers one such possibility. This possibility will be subject of future research. In addition, it will be of interest to

investigate whether the results reported in this paper hold in the more realistic case of a spherical shell. In particular, the spherical case may allow the **add** modes to grow to a much larger amplitude, because geostrophy is not hard-wired into the formulation of the spherical model as it is in the annulus case. If this should be the case, low Rayleigh-number convection may have a more significant role in core dynamics. The influence of imposed magnetic fields and the general parameter dependences of the problem must also be studied in more detail to explore scaling relationships and the possibility of further interesting dynamics.

## Acknowledgements

Discussions with Prof. F.H. Busse, and the suggestions of an anonymous referee are gratefully acknowledged, as is the support of the Royal Society under Research Grant 2010 R2.

## References

- Ardes, M., Busse, F., Wicht, J., 1997. Thermal convection in rotating spherical shells. *Phys. Earth Planet. Inter.* 99, 55–67.
- Braginsky, S., 2006. Formation of the stratified ocean of the core. *Earth Planet. Sci. Lett.* 243, 650–656.
- Braginsky, S., Roberts, P., 1995. Equations governing convection in Earth’s core and the geodynamo. *Geophys. Astrophys. Fluid Dyn.* 79, 1–97.
- Breuer, M., Manglik, A., Wicht, J., Truemper, T., Harder, H., Hansen, U., 2010. Thermochemically driven convection in a rotating spherical shell. *Geophys. J. Int.* 183, 150–162.
- Brummell, N., Hart, J., 1993. High Rayleigh number  $\beta$ -convection. *Geophys. Astrophys. Fluid Dyn.* 68, 85–114.
- Buffett, B., Seagle, C., 2010. Stratification of the top of the core due to chemical interactions with the mantle. *J. Geophys. Res.* 115, B04407.
- Busse, F., Carrigan, C., 1974. Convection induced by centrifugal buoyancy. *J. Fluid Mech.* 62, 579–592.
- Busse, F., Simitev, R., 2011. Remarks on some typical assumptions in dynamo theory. *Geophys. Astrophys. Fluid Dyn.* 105, 234–247.



- Busse, F.H., 1986. Asymptotic theory of convection in rotating cylindrical annulus. *J. Fluid Mech.* 173, 545–556.
- Busse, F.H., 2002a. Convective flows in rapidly rotating spheres and their dynamo action. *Phys. Fluids* 14, 1301–1314.
- Busse, F.H., 2002b. Is low Rayleigh number convection possible in the Earth's core? *Geophys. Res. Lett.* 29, 1105.
- Busse, F.H., Simitev, R., 2006. Parameter dependences of convection driven dynamos in rotating spherical fluid shells. *Geophys. Astrophys. Fluid Dyn.* 100, 341.
- Cardin, P., Olson, P., 1992. An experimental approach to thermochemical convection in the Earth's core. *Geophys. Res. Lett.* 19, 1995–1998.
- Chen, Y., Pearlstein, A., 1989. Stability of free-convection flows of variable-viscosity fluids in vertical and inclined slots. *J. Fluid Mech.* 198, 513–541.
- Fearn, D., Loper, D., 1981. Compositional convection and stratification of Earth's core. *Nature* 289, 393–394.
- Hart, J., 1971. Stability of the flow in a differentially heated inclined box. *J. Fluid Mech.* 47, 547–576.
- Helfrich, G., Kaneshima, S., 2010. Outer-core compositional stratification from observed core wave speed profiles. *Nature* 468, 807–810.
- Huppert, H., Turner, J.S., 1981. Double-diffusive convection. *J. Fluid Mech.* 106, 299–329.
- Jones, C., 2007. Thermal and compositional convection in the outer core, in: Schubert, G. (Ed.), *Treatise on Geophysics*. Elsevier. volume 11, pp. 131–185.
- Kono, M., Roberts, P., 2002. Recent geodynamo simulations and observations of the geomagnetic field. *Rev. Geophys.* 40, 1013.
- Kutzner, C., Christensen, U., 2002. From stable dipolar towards reversing numerical dynamos. *Phys. Earth Planet. Inter.* 131, 29–45.
- Lister, J., Buffett, B., 1995. The strength and efficiency of thermal and compositional convection in the geodynamo. *Phys. Earth Planet. Int.* 91, 17–30.
- Manglik, A., Wicht, J., Christensen, U.R., 2010. A dynamo model with double diffusive convection for Mercury's core. *Earth and Planet. Sci. Lett.* 289, 619–628.
- Meseguer, A., Marques, F., 2002. On the competition between centrifugal and shear instability in spiral poiseuille flow. *J. Fluid Mech.* 455, 129–148.
- Nimmo, F., 2007. Energetics of the core. In: Schubert, G. (Ed), *Treatise on Geophysics*, vol. 8, Elsevier, 31–65.
- Or, A., Busse, F., 1987. Convection in a rotating cylindrical annulus. Part 2. Transitions to asymmetric and vacillating flow. *J. Fluid Mech.* 174, 313–326.
- Pearlstein, A., 1981. Effect of rotation on the stability of a doubly diffusive fluid layer. *J. Fluid Mech.* 103, 389–412.
- Plaut, E., Busse, F., 2002. Low-Prandtl-number convection in a rotating cylindrical annulus. *J. Fluid Mech.* 464, 345–363.
- Plaut, E., Busse, F., 2005. Multicellular convection in rotating annuli. *J. Fluid Mech.* 528, 119–133.
- Plaut, E., Lebranchu, Y., Simitev, R., Busse, F.H., 2008. Reynolds stresses and mean fields generated by pure waves: applications to shear flows and convection in a rotating shell. *J. Fluid Mech.* 602, 303–326.
- Sakuraba, A., Roberts, P., 2009. Generation of a strong magnetic field using uniform heat flux at the surface of the core. *Nature Geosci.* 2, 802–805.
- Schmitt, R., 1994. Double diffusion in oceanography. *Annu. Rev. Fluid Mech.* 26, 255–285.
- Schnaubelt, M., Busse, F., 1992. Convection in a rotating cylindrical annulus. Part 3. Vacillating and spatially modulated flows. *J. Fluid Mech.* 245, 155–173.
- Simitev, R., Busse, F.H., 2005. Prandtl number dependence of convection driven dynamos in rotating spherical fluid shells. *J. Fluid Mech.* 532, 365–388.
- Stanley, S., Mohammadi, A., 2008. Effects of an outer thin stably stratified layer on planetary dynamos. *Phys. Earth Planet. Int.* 168, 179–190.
- Straughan, B., Walker, D., 1997. Multi-component diffusion and penetrative convection. *Fluid Dyn. Res.* 19, 77–89.
- Takehiro, S.I., Yamada, M., Hayashi, Y.Y., 2010. Retrograde equatorial surface flows generated by thermal convection confined under a stably stratified layer in a rapidly rotating spherical shell. *Geophys. Astrophys. Fluid Dyn.* DOI: 10.1080/03091929.2010.512559.
- Turner, J.S., 1974. Double-diffusive phenomena. *Ann. Rev. Fluid Mech.* 6, 37–54.
- Turner, J.S., 1985. Multicomponent convection. *Ann. Rev. Fluid Mech.* 17, 11–44.